catalysts

MDPI

Review

Single-Atom Transition Metal Photocatalysts for Hydrogen Evolution Reactions

Thang Phan Nguyen and Il Tae Kim *

Department of Chemical and Biological Engineering, Gachon University, Seongnam-si 13120, Gyeonggi-do, Korea
* Correspondence: itkim@gachon.ac.kr

Abstract: Hydrogen is one of the potential fuels that is easily stored in ammonia compounds and reacts with oxygen in an environmentally friendly manner, producing water and transferring a significant amount of heat for powering mechanical facilities or transportation. Recently, single-atom photocatalysts have attracted significant attention owing to their ability to produce clean fuels or reduce gaseous pollution, thereby contributing to the preservation of our planet. Utilizing metals composed of a single atom on a semiconductor platform can improve the active sites, thereby increasing the efficiency of the hydrogen evolution reaction. This review focuses on the use of single-atom transition metals as photocatalysts in a solar-powered water-splitting system that produces hydrogen gas. The approach to synthesis, reaction mechanism, and current performance of these materials is exhaustively discussed. In addition, the main challenges and improvement strategies are highlighted.

Keywords: single-atom; transition metal; hydrogen evolution reaction; photocatalyst; semiconductor

Citation: Nguyen, T.P.; Kim, I.T. Single-Atom Transition Metal Photocatalysts for Hydrogen Evolution Reactions. *Catalysts* **2022**, *12*, 1304. https://doi.org/10.3390/catal12111304

Academic Editor: Pankaj Raizada

Received: 8 September 2022
Accepted: 21 October 2022
Published: 24 October 2022

1. Introduction

The impending depletion and negative environmental effects of fossil fuels necessitate a vast supply of renewable energy sources for human life and industry. Hydrogen (H_2) is considered as a potential renewable energy source owing to its abundance, high energy density, and environmental friendliness [1–3]. In addition, hydrogen plays an important role in numerous applications, including fuel, oil refinery, fertilizer, and metal refining. Figure 1 illustrates solar hydrogen production and its applications. Using solar energy, the photocatalyst absorbs photons to produce excited electrons that can combine with a proton to produce hydrogen gas. This approach is sustainable and can satisfy the demand for a large-scale, low-cost hydrogen generation system [4,5]. H_2 possesses the lightest weight, the strongest reaction with oxygen that produces water, and a tremendous amount of heat energy, allowing it to operate machinery or generate electricity via a converter [6]. The majority of hydrogen gas is produced by methane steam reforming or oil reforming, but water splitting is significantly less expensive, requires fewer facilities, consumes renewable solar energy, and emits non-toxic by-products [7–9]. Therefore, the development of this sustainable energy pathway is the optimal choice for the energy economy of the future.

Protons (H^+) receive an electron to produce hydrogen, resulting in the formation of hydrogen gas and formation of a bubble on the surface of materials [10]. This reaction depends on the redox potential of H^+/H_2, and the active proton source depends on the pH of the electrolyte, where the protons are from the free H^+ in acidic media or the H_2O molecule in basic media [11–14]. For example, in the acidic media (pH < 5), the protons are directly absorbed on the surface of material, receive the electrons, and are reduced to hydrogen. Meanwhile, in basic media (pH > 8), the protons are separated from water molecules on the surface of active material. Therefore, the water splitting potential depends on the pH level; the HER potential is 0 V vs. standard hydrogen electrode (SHE) at pH = 0, while it is −0.83 V vs. SHE at pH = 14 [15,16]. This change can be calculated as a function

of pH; thus, to simplify the reaction, we can mention the behaviour of the adsorbed H^+ (namely, H_{ads}). Accordingly, the adsorption ability determines the performance of the hydrogen evolution reaction (HER). The main active material in single-atom photocatalysts is the light harvester, a semiconductor, which absorbs visible light or UV light and then excites the formation of electron-hole pairs, producing an electron source for HER [17]. Excited electrons with higher energy than the band gap of the semiconductor will transfer to the conduction band, while the holes remain in the valence band or join in an oxidation reaction [18]. By selecting a semiconductor with a conduction band close to the H^+/H_2 reduction level of ~4.5 eV (or 0 V vs. SHE), protons can receive electrons from host materials with relative ease. This is how conventional photocatalysts function [19,20].

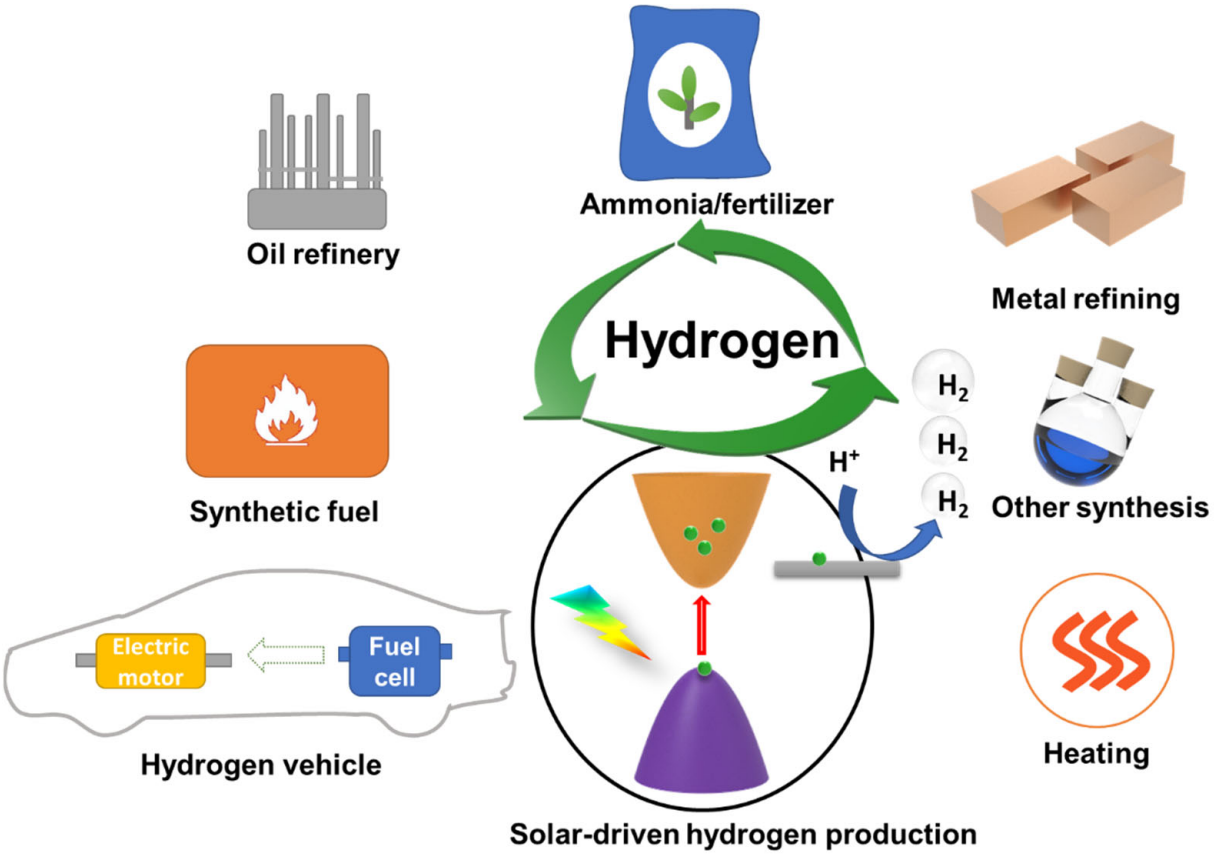

Figure 1. Solar-driven hydrogen production and hydrogen applications.

Recently, single-metal atom (SMA) photocatalysts have attracted considerable interest [21–23]. The term of SMA photocatalyst indicates the decoration of a very tiny metal particle in atomic scale on the host photocatalyst (semiconductors). The single metal functions as a co-catalyst on the surface of semiconductors, increasing the number of active sites, receiving electrons from the light-harvesting process, and efficiently reducing the amount of precious metal. Typically, precious metals such as Pt and Au have a low work function that is close to the H^+/H_2 reduction level; as a result, they have been utilized as hydrogen catalysts in electrochemical and photoelectrochemical hydrogen generation [24]. Due to the Schottky contact between the metal atom and semiconductor host material, the electron can easily transfer to a lower potential and is able to donate electrons to H_{abs}, thereby forming hydrogen molecules [25,26]. Common semiconductor hosts include perovskites, TiO_2, and NiO, as well as graphitic carbon nitride (g-C_3N_4) [27]. Meanwhile, to reduce the expense of precious metals, numerous types of abundant transition metals such as Pt, Au, Ni, V, and Fe are used to produce SMA photocatalysts [28–31].

In this review, the use of transition metal as a single-atom photocatalyst is examined. In addition, the fundamentals and predictions based on theoretical calculations are discussed, and the evaluation, recent developments, and future prospects are discussed.

2. Fundamentals

Typically, the SMA photocatalyst consists of a single metal atom or tiny metal nanoparticle anchored on a host material, as shown in Figure 2a. The host material is semiconductor-type material, which itself can act as a photocatalyst or light harvesting material [21]. As mentioned above, the requirement of active material for HER should have a conduction band close to ~4.5 eV. However, it is hard to tune a band gap of semiconductors as designed. For metal, the conduction band and valence band are overlapped or have no band gap. Therefore, the electron and hole are easily formed in normal conditions. As per previous reports, the work function of metal can be understood by the "activity descriptors" [32]. Thus, Pt with the work function of ~5.5 eV seems to be the best element to effectively perform HER [24]. In fact, many other factors of transition metal affect HER performance, which will be discussed later. To operate the HER, the transition metal nano particle should be anchored on semiconductor material, as described in the schematic in Figure 2a; the host material acts as the light harvester, then gives the generated electrons to metal NPs. The tiny metal NPs receive the electron and perform the HER, producing H_2 gas. Due to the natural catalytic activity and the increasing surface area of metal nanoparticles, photocatalytic properties of SMA can enhance outstanding photocatalytic properties of bare semiconductor material [33].

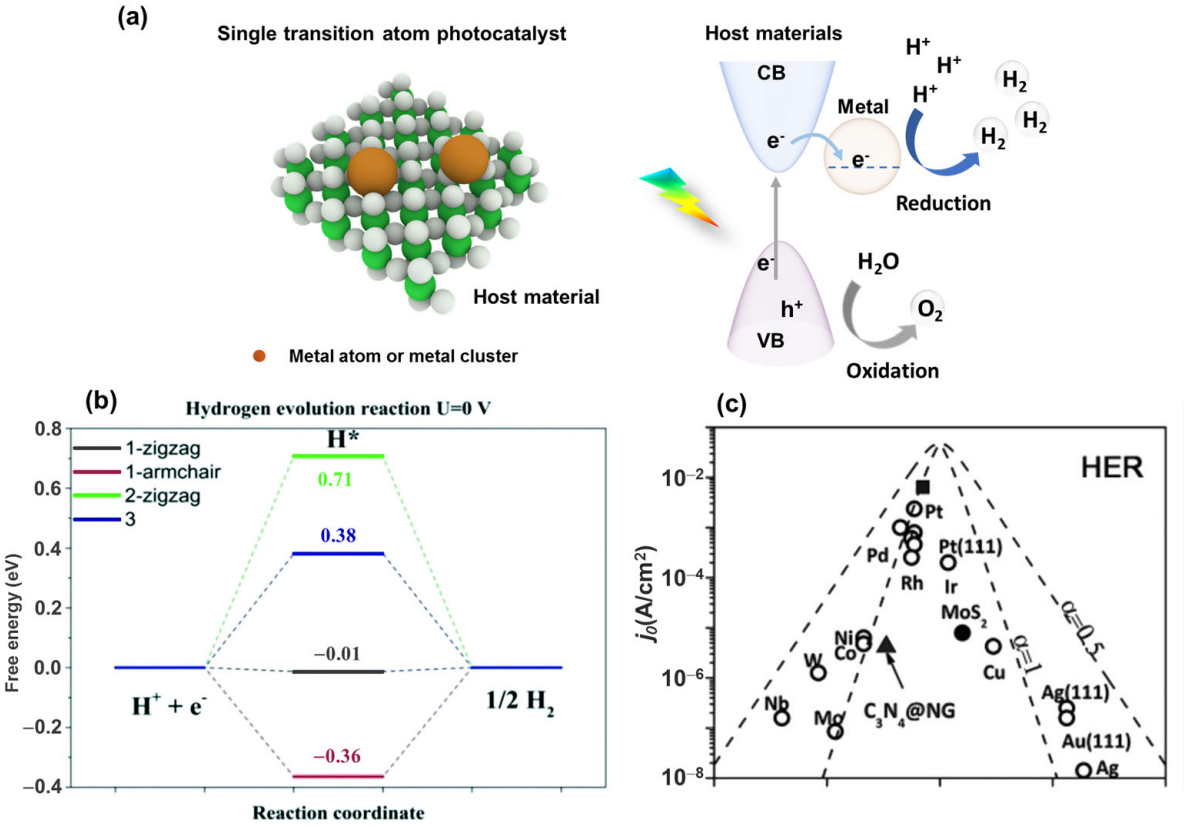

Figure 2. (**a**) The structure of single transition metal atom (SMA) photocatalyst and scheme of SMA photocatalyst in hydrogen evolution reaction. (**b**) Gibbs free energy for hydrogen evolution reaction (HER) at different coordination sites of Ni. Reproduced with permission from ref. [34] with permission from the Royal Society of Chemistry. (**c**) Dependence of exchange current density (j_0) on the ΔG_{H*} of the surface of various metals. Reproduced with permission from ref. [35] Copyright 2015, Wiley-VCH.

To fully comprehend the mechanism of hydrogen absorption and reduction on the surface of a transition metal, the density functional theory (DFT) calculation can be used to gain insight into the electron structure, particularly the d-orbital of the transition metal, which determines the conducting electron energy [10,36–38]. After adsorption on the material surface, the proton forms a bonding state that can be described as a 1s-d hydrogen-transition metal bond. Hammer et al. reported that the density of one-electron states (DOS) of four typical metals in this group, including Pt, Au, Ni, and Cu, were calculated to predict the chemisorbed hydrogen on their surfaces [39]. Au and Cu have electrons in their H 1s-d antibonding states, while those of Ni and Pt are empty. It indicates that metals interact more strongly with H_{ads} of Ni and Pt than with H_{ads} of Au and Cu. However, the H 1s-d bonding in both these transition metals shows a strong intensity, indicating they can highly absorb the hydrogen atom. Therefore, the position and occupation of d-orbitals determine the hydrogen adsorption properties of metal surfaces. In HER, the bond-breaking barrier and the electron transfer process are also essential [40]. Metals appear to have the lowest bond-breaking barrier, allowing them to readily transfer electrons and activate hydrogen in HER. Thus, the use of metal atoms such as Pt, Au, Pd, Co, Ni, and Cu in photocatalyst systems will reduce the massive electron transfer effort of the semiconductor, resulting in more efficient hydrogen production.

The ability to absorb hydrogen can be described by a physical quantity called Gibbs free energy (ΔG_{H*}) [41,42]. The value of ΔG_{H*} is more negative, indicating that hydrogen bonds to the surface more strongly. The greater the positive value, the more difficult it is to absorb hydrogen. Thus, the material with the closest value to zero for ΔG_{H*} is the best material for interacting with hydrogen atoms with the lowest activation energy, as it can absorb and release the proton and hydrogen gas, respectively, with ease. Figure 2b depicts the typical free energy diagram of Ni metal at various sites [34]. The Ni 1-zigzag edge has the lowest ΔG_{H*} value of -0.01 eV, indicating HER's high activity. In contrast, the other coordinated sites exhibit either strong or very weak hydrogen bonds, making hydrogen absorption difficult. By repeating the calculation with other transition metals, such as Mn, Fe, Co, Ni, Cu, and Pd, Gao et al. obtained a clear picture of these materials in which, if the right coordinated sites are exposed in the bonding with photocatalyst active sites, they are both highly active in HER [34]. Figure 2c displays the volcano plots of Gibbs free energy for the majority of transition metals (Pt, Au, Pd, Rh, Ir, Ni, Co, Mo, Nb, W, Ag), which were summarized by Yao et al. using previously reported data [35,43–46]. It is easy to evaluate transition metals for hydrogen adsorption based on this graph. However, as stated previously, the Gibbs free energy of a metallic surface is highly dependent on its coordinated sites. Therefore, a graph with numerous coordinated sites must be completely filled to provide an overview of transition metal in HER.

3. Single-Atom Metal Photocatalyst Preparation

To synthesize single-atom photocatalysts, numerous techniques can be used, which can be categorized into three approaches: Absorption, deposition, and refining method (as shown in Figure 3). In the absorption method, metallic salts were absorbed by a structure, such as a metal organic framework (MOF), a polymer structure, or a mixture of precursors of host materials. Zhang et al., for instance, fabricated a few types of SMAs, including Cu, Co, Ni, Fe, Mn, Zn, and Pt, by diffusing these ions into a MIL-125-Ti, which is an MOF structure of Ti with terephthalic acid, and then reducing this structure to SMA on TiO_2 host structure as a photocatalyst for hydrogen production [47]. Cha et al. used TiO_2 dissolved in Pt, Pd, and Au chlorides [48]. The absorption of these ions on the surface of TiO_2 produces 2–5 nm-sized particles that are considered atomic-scale catalysts. The atomic deposition technique permits a single atom to exist on the surface of materials within seconds. Pan et al. investigated the electrostatic deposition method for SMA Ni particle on $ZnIn_2S_4$, as an example [49]. Due to the large surface area of $ZnIn_2S_4$, Ni^{2+} ions are readily attracted to the material via electronic attraction. By hydrothermally reducing Ni^{2+}, the SMA Ni particle was uniformly decorated on the surface of the host material.

Meanwhile, Zhou et al. employed a three-electrode system and a solution of H_2PtCl_6 as a Pt source for electrodeposition on Ni/NiO/Ag nanowire [50]. The amount of Pt particles can be manipulated by adjusting the time and current/voltage of the electrodes system. In the final step of the refining method, metal ions were reduced through a natural decomposition process under light/dark conditions (with light-sensitive compounds of Pt, Ag, and Au) or through the use of reduction agents such as hydrogen or calcination with a reducing agent. Vile et al. applied sodium borohydride to C_3N_4 nanosheets to reduce Ni^{2+} [51]. Additionally, Zhang et al. used a high annealing temperature of ~850 °C to decompose cobalt phthalocyanine in a composition containing carbon black in the presence of nitrogen [52]. Moreover, Zhou et al. used the self-decomposition of $IrCl_3$ in the absence of light to produce single-atom Ir on TiO_2 nanotubes [53]. Table 1 provides a summary of additional methods. Approaching the synthesis of SMA photocatalysts may not be a simple process, but it is not an impediment to obtaining the desired photocatalysts.

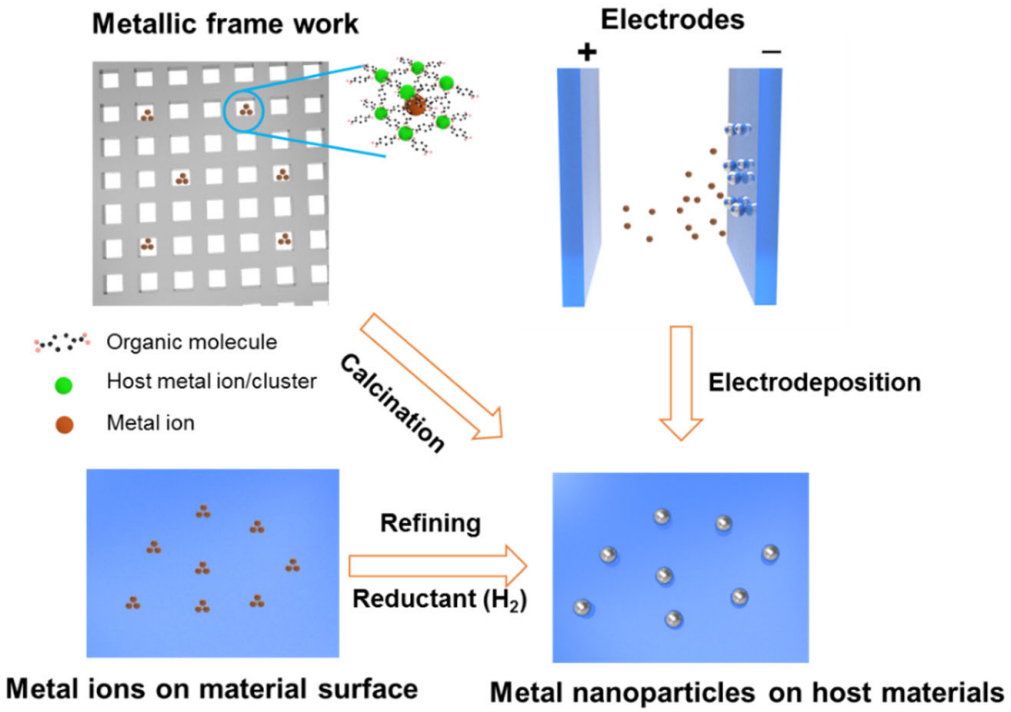

Figure 3. Synthesis of the single-metal atom photocatalysts.

Table 1. Summarization of synthesis approaches for SMA photocatalyst.

Single-Atom Metal	Host Materials	Synthesis Method	Ref
Cu, Co, Ni, Fe, Mn, Zn, Pt	TiO_2	Absorption on MOF and calcination	[47]
Ni	TiO_2	Refining by hydrothermal	[54]
Ni	$ZnIn_2S_4$	Deposition: electrostatic deposition + hydrothermal	[49]
Pd, Pt, Au	TiO_2	Absorption: Immersing in salts	[48]
Ni	C_3N_4	Refining by sodium borohydride	[51]
Co	N-Carbon	Refining by calcination	[52]
Pt	Ni/NiO on Ag NWs	Electrodeposition	[50]
V	C_3N_4	Refining by calcination	[55]
Ir	TiO_2	Deposition in dark	[53]
Pt	Graphene	Deposition: Atomic layer deposition	[56]
Cu	BN	Refining by calcination	[57]

4. Single-Atom Photocatalysts

4.1. TiO_2 Base

TiO_2 is a well-known photocatalyst with a wide band gap of ~3.2 eV that absorbs ultraviolet light intensely (UV) [58,59]. In addition, it has been used globally for numerous applications, including batteries, ceramic compounds, colorants, and solar cells, owing to its low cost, low toxicity to the environment, and ease of processing [60–62]. As a hydrogen photocatalyst, TiO_2 shows a low efficiency due to the ultrafast recombination of excited electron–hole pairs [63]. Correspondingly, the morphology and size of TiO_2 can be altered to improve its catalytic performance [62,64]. However, to reach the large-scale production requirement, there is still a gap to overcome. Numerous strategies aim to modify the TiO_2 surface, including the use of semiconductors with a smaller band gap and the combination of metal particles and graphene, among others. Both received a tremendous performance boost from TiO_2. In particular, the use of SMA on photocatalysts opens a new route for functionalizing the TiO_2 surface with tiny metal particles.

Figure 4a,b demonstrates that Yi et al. synthesized single-atom Co on N-doped graphene composited with TiO_2 nanobelts, resulting in a significant improvement [65]. The rate of H_2 generation could reach ~677 $\mu molh^{-1}$ g^{-1}, which is comparable to the performance of Pt-decorated TiO_2 samples (~741 $\mu molh^{-1}$ g^{-1}). Meanwhile, the hydrogen production efficiency of unmodified TiO_2 and N-doped graphene/TiO_2 is poor and low, respectively. Using a similar approach, Cha et al. compared the effect of using the noble metals Pt, Pd, and Au on the surface of TiO_2, as depicted in Figure 4c,d [48]. The size of tiny noble metals was between 2 and 5 nm. By adjusting the concentration of noble metal chlorides, it is possible to observe the effect of SMA on TiO_2 host material, which demonstrates that a single atom can enhance the performance of photocatalysts by increasing the number of active sites, without obstructing the light to the host material compared to larger nanoparticles. The best performance as an SMA photocatalyst was recorded for Pd, which has a hydrogen production rate of ~600 μLh^{-1}. Zhou et al. deposited Ir on TiO_2 nanotubes using a dark deposition technique, loading the nanotubes with Ir nanoparticles measuring ~2.5 nm in size [53]. The SMA on TiO_2 photocatalyst performs significantly better than the conventionally prepared co-catalyst TiO_2, achieving a high turnover frequency of ~4×10^6 h^{-1}. Zhang et al. reported the SMA Cu on TiO_2, as depicted in Figure 5, after selecting a material with a lower cost [47]. The trapped Cu^{2+} ion in MIL125-Ti was easily converted to SMA Cu/TiO_2 via high-temperature calcination. By comparing various types of transition metals, such as Co, Ni, Fe, Mn, Zn, and Pt, the author concluded that single atom Cu (~2 nm) on TiO_2 possesses a high H_2 evolution rate of ~100 $mmolh^{-1}$ g^{-1}, which is higher than that of SMA Pt on TiO_2 (~80 $mmolh^{-1}$ g^{-1}). The significant improvement of these SMA photocatalysts can be attributed to two factors. First, the new approach using MIL-125-Ti demonstrates that an MOF can absorb other ions efficiently if their ionic size and repulsion/attraction force are suitable. In this work, Cu is abundantly absorbed by the network, resulting in the formation of 1–2 atomic-sized uniform single atoms. Cu is a well-known metal that is utilized in HERs effectively due to its compatibility with the H^+/H_2 redox potential. The disintegration of MIL-125-Ti also generates a large number of Ti vacancies, thereby increasing the specific surface area and exposing sites for Cu atoms. Therefore, the use of SMA in conjunction with a highly porous host material can increase the efficiency of hydrogen generation.

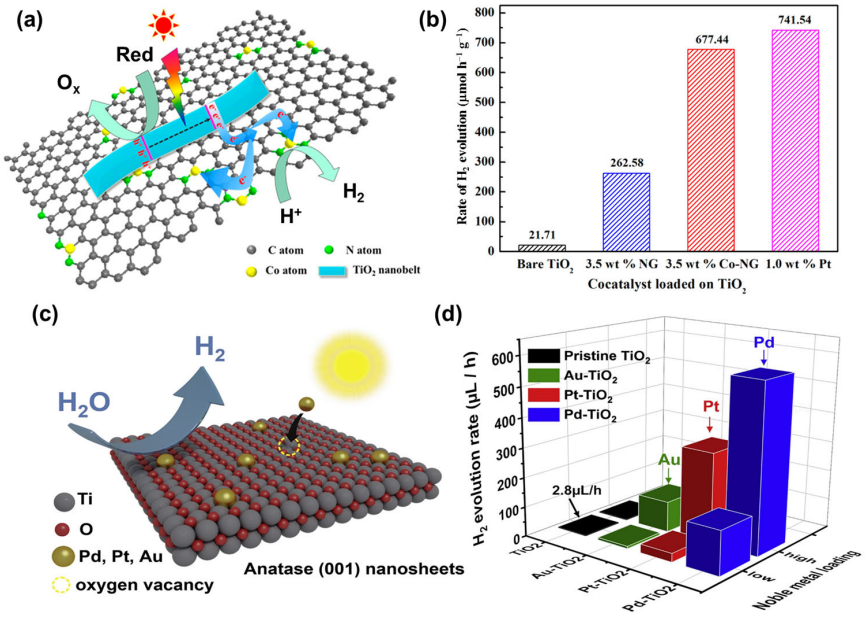

Figure 4. (**a**) Schematic for photocatalytic reaction of TiO_2 nanobelts on N-graphene, (**b**) H_2 evolution rate of TiO_2 nanobelts and composites. Reprinted with permission from ref. [65] Copyright 2018, American Chemical Society; (**c**) illustration of noble metal on anatase (001) TiO_2 nanosheets and (**d**) photocatalytic H_2 evolution rate of noble metal on TiO_2 nanosheets. Reproduced with permission from ref. [48] Copyright 2021, Elsevier.

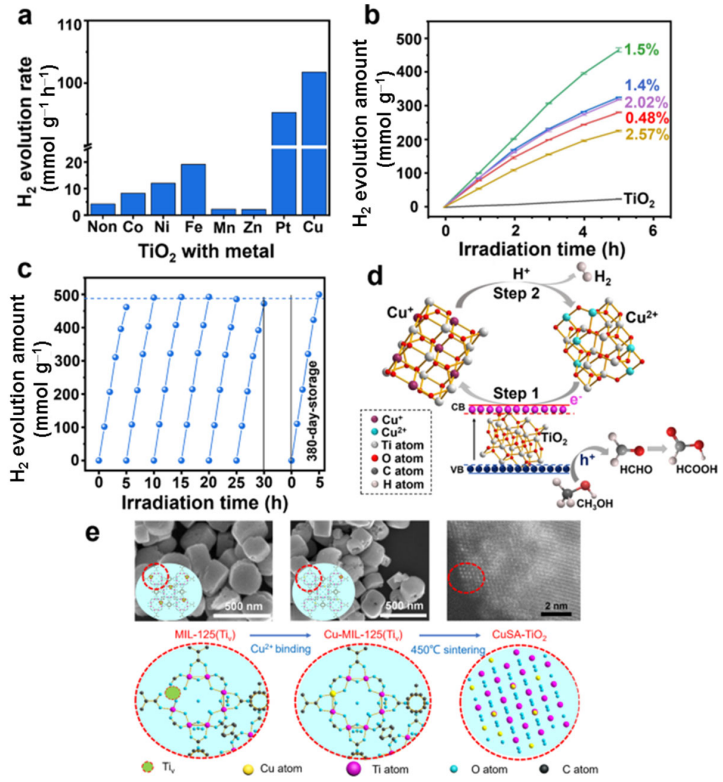

Figure 5. (**a**) The photocatalytic H_2 evolution rate of bare TiO_2 and SMA TiO_2 with different metals; (**b**) H_2 production of bare TiO_2 and SMA TiO_2 with different amount of Cu; (**c**) with 1.5 wt.% Cu SA-TiO_2 for 380 days; (**d**) the photocatalytic H_2 evolution mechanism on Cu SA-TiO_2; and (**e**) the corresponding schematic representation of the formation of copper SMA in the lattice of TiO_2, corresponds to their electron images. Reproduced with permission from ref. [47] Copyright 2022, Springer Nature.

4.2. g-C_3N_4 Base

Graphitic carbon nitride (g-C_3N_4), a two-dimensional layered material that is a member of the graphene-like family, is an efficient metal-free photocatalyst material [66]. In contrast to graphene, which has a zero band gap, g-C_3N_4 has a band gap of ~2–3 eV [67,68]. Consequently, g-C_3N_4 has a broad light absorption band. In addition, g-C_3N_4 has a simple synthesis method, high physical and chemical stability, and an active band gap in relation to the redox potential of water-splitting reaction [69]. Therefore, g-C_3N_4 materials can be utilized as photocatalysts for HER. However, due to its low conductivity and rapid recombination of excited charge carriers, g-C_3N_4 is ineffective as a photocatalyst [70]. Accordingly, surface engineering of g-C_3N_4 is required to overcome the limitation and exploit the semiconducting properties effectively. Due to the abundance of nitrogen atoms in its structure, the surface of g-C_3N_4 can be easily modified by covalent or noncovalent bonding with a variety of functional groups [71]. During its early use as a photocatalyst, the metal decoration in the surface of g-C_3N_4 has garnered considerable attraction [72,73]. The emergence of SMA properties on the host photocatalyst material g-C_3N_4 can have a substantial impact on their hydrogen production performance. Cao et al. utilized a single atom of noble Pt metal on g-C_3N_4 as an effective photocatalyst in HER, as depicted in Figure 6a–b [74]. The Pt atoms are widely distributed on the host surface materials as individual atoms, thereby enhancing the active site and photocatalytic properties. Pt is used not only to increase the active surface area but also to improve the electronic conducting property, resulting in outstanding catalytic properties. The hydrogen production rate of SA Pt on g-C_3N_4 is significantly greater than that of bare g-C_3N_4 and greater than 13 times that of Pt nanoparticles of larger size (a few nanometers) on g-C_3N_4. In addition to V, Co, Cu, and Fe, other transition metals are used in the single atomic concept of g-C_3N_4. To display a wider graph of SMA on g-C_3N_4, however, the synthesis approach still has some limitations. Li et al. fabricated SMA Co metal on P-doped g-C_3N_4 (Co/P/CN) using hexahydrate triethanolamine as a reducing agent during the calcination process in a microwave reactor, as depicted in Figure 6c,d [75]. The rate of H_2 production was measured at ~3730 $\mu molh^{-1}$ g^{-1}. The addition of Co and P atoms to g-C_3N_4 increases its active surface area. Consequently, the presence of P-N and Co-N bindings causes a change in the band gap structure, which is reduced from ~2.78 eV for bare g-C_3N_4 to ~2.58 eV for Co/P/CN, as depicted in Figure 6c. Therefore, the photogenerated hole–electron pairs could easily separate and contribute to the HER. Similarly, Wang et al. reduced V ion during the preparation of g-C_3N_4, resulting in a single atom of V on g-C_3N_4 photocatalyst (SAVCN) for hydrogen evolution reaction (Figure 6e,f) [55]. Additionally, the simulations demonstrated that the V on SAVCN decreases the ΔG_{H*} from -1.11 to -0.34 eV, which is closer to 0 eV and therefore better for hydrogen adsorption. Under blue and green LED lights, the H_2 production capacity of the SAVCN catalyst was measured and found to be ~5.0 and 3.0 $mmolh^{-1}$ g^{-1}, respectively. Consequently, the SMA improved the light absorption, hydrogen adsorption, and band gap structure of the host material to facilitate the HER.

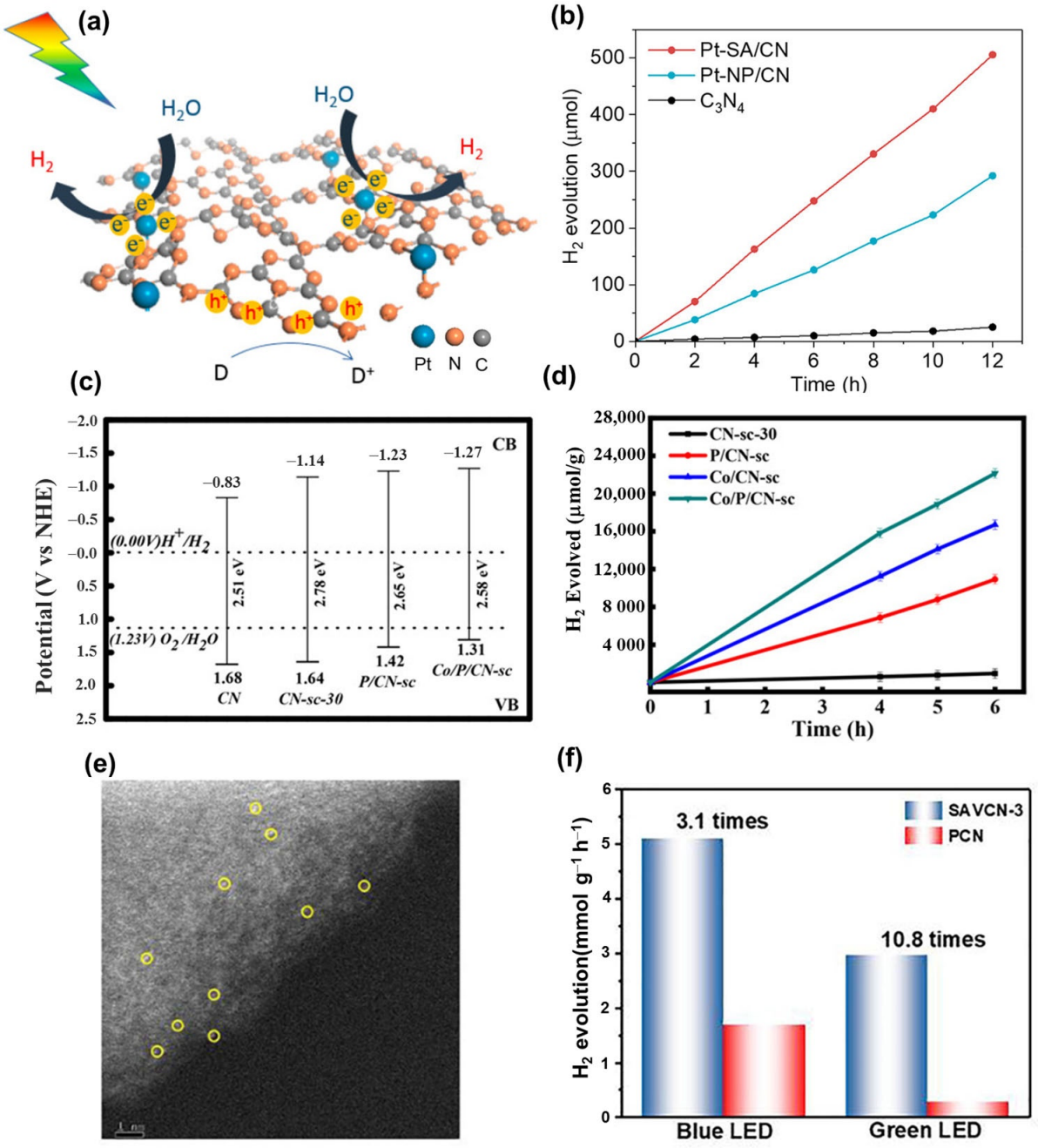

Figure 6. (**a**) Illustration of the photocatalytic mechanism on Pt SMA on g-C_3N_4; (**b**) H_2 evolution of Pt SMA on g-C_3N_4 compared with Pt nanoparticle and bare C_3N_4 samples. Reprinted with permission from ref. [74] Copyright 2018, American Chemical Society. (**c**) Electronic band structures and (**d**) H_2 evolution of the as-prepared g-C_3N_4 and SMA g-C_3N_4 samples. Reproduced with permission from ref. [75] Copyright 2021, American Chemical Society. (**e**) Spherical aberration-corrected HAADF-STEM image of the SMA on ultrathin C_3N_4 (SAVCN) and (**f**) hydrogen production rate under blue/green LED of polymeric C_3N_4 (PCN) and SAVCN samples. Reproduced with permission from ref. [55] Copyright 2022, Elsevier.

4.3. Other Host Materials

In addition to TiO_2 and g-C_3N_4, which are the traditional photocatalyst host materials, there are numerous other semiconductor materials whose band gap matches the requirements for a photocatalyst material [76]. However, their use is contingent on their influence on low-cost production, simple processing, and environmentally friendly properties, which are not adequately accounted for by their benefits and drawbacks. Graphene quantum dots, for instance, are one of the most promising candidates; however, large-scale production and uniformity are still being evaluated [23]. Due to their layered structure, photo-stability, low band gap of ~2.5 eV, and low toxicity, $ZnIn_2S_4$ semiconductor materials have recently attracted the attention of researchers [77–79]. To date, Pan et al. investigated the SMA Ni on $ZnIn_2S_4$ materials for HER, as shown in Figure 7a,b [49]. Preparing a $ZnIn_2S_4$ semiconductor with sulphur vacancies and synergizing it with SMA Ni on the surface enabled the photocatalytic evolution of hydrogen. The evolution rate with 0.9 wt.% Ni on $ZnIn_2S_4$ was approximately 89.4 μmolh^{-1}. Shi et al. fabricated SMA Pt on hexagonal $ZnIn_2S_4$ [80]. Calculating a new ΔG_{H*} at −0.23 eV for the third hydrogen atoms demonstrated that the presence of Pt increases the hydrogen adsorption of the photocatalyst. Under solar light, the rate of hydrogen production was approximately 30 mmolg^{-1} h^{-1}, and under visible light, it was greater than 16 mmolg^{-1} h^{-1}. These outcomes suggest $ZnIn_2S_4$ bearing SMA coating is also a possible photocatalyst for hydrogen production.

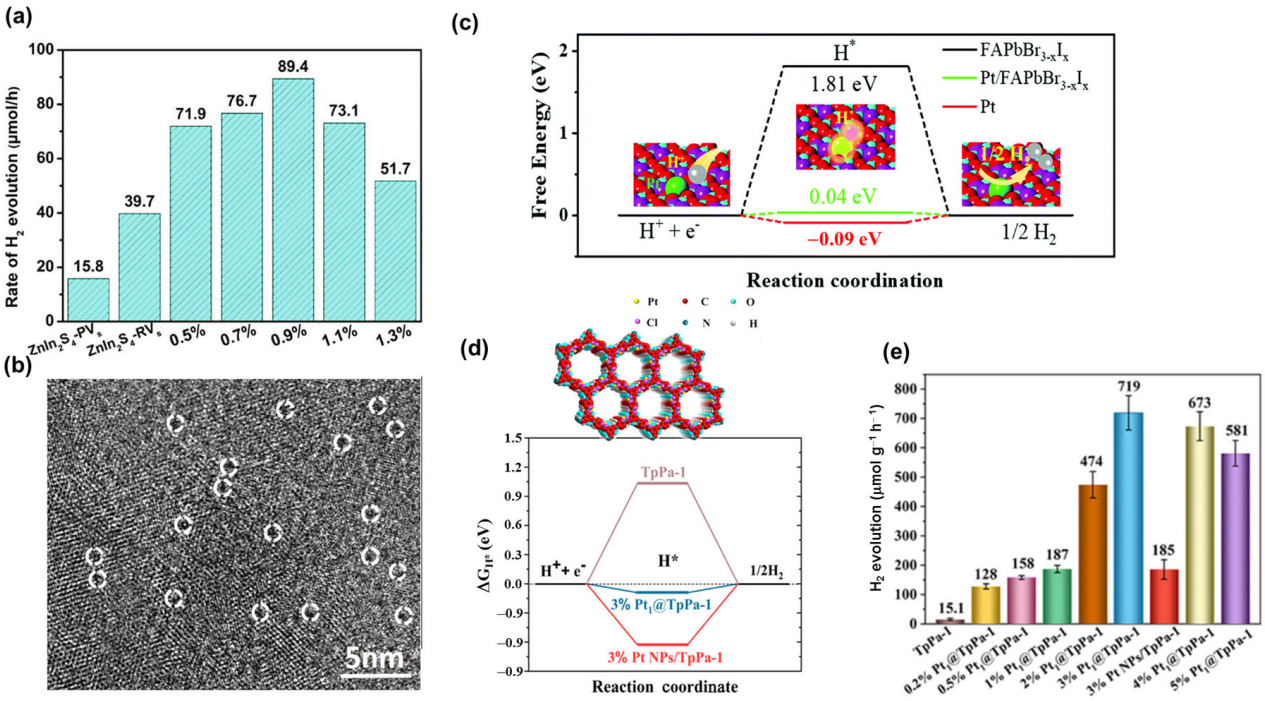

Figure 7. (**a**) H_2 evolution rates of $ZnIn_2S_4$ with different weight ratios of Ni co-catalyst and (**b**) HRTEM image showing Ni single atom (0.9%) on $ZnIn_2S_4$. Reproduced with permission from ref. [49] Copyright 2021, Elsevier. (**c**) Calculated Gibbs free energy of H* adsorption for Pt, FA perovskite with and without Pt SMA. Reproduced with permission from ref. [81] Copyright 2022, Royal Society of Chemistry. (**d**) Calculated Gibbs free energy of H* adsorption with an illustration of TpPa-1-COF; and (**e**) H_2 evolution rate of TpPa-1-COF with different amounts of Pt SMA. Reproduced with permission from ref. [82] Copyright 2021, American Chemical Society.

Organometal halide perovskites (OHP) are well-known in the solar cell industry due to their tuneable band gap, broad light absorption band, long carrier diffusion length, and simple synthesis [83]. In particular, the photocatalytic splitting of hydroiodic acid (HI) in aqueous solution promotes the solar-powered production of hydrogen [84–90]. Zhou et al. identified Cs_2SnI_6 perovskites combined with SMA Pt as a promising candidate

for the treatment of HER [91]. The Pt-I_3 sites were proposed to have a strong metal-support interaction effect, enhancing the photocatalytic performance of HER. Wu et al. also utilized a single Pt atom on a formamidinium (FA)-based lead perovskite containing Br and I atoms [81]. The FA perovskites have a small band gap and halide mixture, which increases their stability and light absorption, as illustrated in Figure 7c. Pt on FA perovskites exhibited a ΔG_{H*} of ~0.04 eV, which is suitable for the adsorption of hydrogen atoms and the subsequent release of hydrogen gas. Approximately 700 $\mu molh^{-1}$ of hydrogen was produced. From light-harvesting materials, OHP with SMA could be a candidate for hydrogen production and other photocatalytic applications.

In addition to conventional semiconductors, the 2D structure, high stability, and catalytic properties of covalent organic frameworks (COFs) make them attractive for photocatalyst systems [92–100]. High catalytic performance is exhibited by COFs containing transition metals when reducing the toxic organic chemical CO_2 or producing hydrogen. For example, Zhong et al. synthesized single Ni site COFs for CO_2 and H_2 production [95]. The COFs were produced using a solvothermal method involving 1,3,5-triformylphloroglucinol and 5,5′-diamino-2,2′-bipyridine, resulting in a material that is stable and more selective for CO_2 reduction than HER. In COFs, the selected metal and framework play a greater role in determining their catalytic properties. Dong et al. used a Pt single atom in β-ketoenamine-linked COFs (Pt-SA-TPa-1-COFs), as shown in Figure 7d,e [82]. The 2D Pt-SA-TPa-1-COFs exhibit numerous active sites and a low band gap of ~2.0 eV, resulting in a strong absorption of visible light from ~550 nm to the near IR band. Consequently, the calculation of ΔG_{H*} reveals a low energy of –0.092 eV, activating the hydrogen adsorption property and encouraging the release of H_2 following production. Pt-SA-TPa-1-COFs can generate hydrogen at a rate of 719 $\mu molh^{-1}$ g^{-1}. With an SMA on the surface, the development of semiconductors is accelerating. Accordingly, numerous semiconductor laboratories are employing this approach to identify the most effective catalyst activator for OER, HER, CO_2 reduction, and organic reduction. They can be metal oxide material, MOF, metal sulphides, metal selenides, etc. [50,101–106].

To evaluate the performance of different materials, Table 2 shows the summary of the single atom photocatalyst for hydrogen evolution reaction with various metals and host materials. It can be clearly recognized that in each host material, the different transition metal shows the different behaviour. In general, the presence of transition metal can improve the catalytic properties of host material. This is because free electron can be easily generated and transferred from host material to give it to H_{ads}. Pt is the most common metal for enhancing catalytic performance, due to its natural catalytic properties [74]. However, the abundance and price of Pt limits its commerciality. Therefore, Cu, Ni, and Co are the next candidates for Pt replacement [47,107]. Moreover, the host materials in nano scale, such as nanosheets, nanobelts, or particles, are generally utilized. It is worth noting that a high surface area is a prerequisite for a light harvester. In Table 2, the TiO_2 is derived from MIL125-Ti structure, which can achieve a high surface area from the collapse of this framework. Therefore, it can boost the hydrogen production up to ~100 mmol g^{-1} h^{-1} [47]. Moreover, the use of Cu in TiO_2 shows a better performance in comparison to Pt. This indicates that the suitable structure and metal can generate a synergistic effect for their catalytic properties. Therefore, host materials in the right form with metals are promising to be a future active material for hydrogen production.

Table 2. Comparison of various kinds of catalyst with/without single transition metal atom for hydrogen evolution reaction.

Metal Atom	Host Materials	Photocurrent (μA cm^{-2})	H_2 Evolution Rate (mmol $g^{-1} \cdot h^{-1}$)	Reference
Co -	TiO_2 nanobelt	~83 ~28	~0.677 ~0.0217	[65]
Co Ni -	TiO_2 nanosheets (NSs)	n/a n/a n/a	~2.9 ~1.0 ~0.04	[107]
Cu Pt -	TiO_2 (derived from MIL125-Ti)	~3.0 n/a ~1.0	~101.7 ~95.0 ~4.2	[47]
Pt -	g-C_3N_4 NSs	n/a n/a	~0.042 ~0.001	[74]
Co -	P-doped C_3N_4 ultrathin NSs	6.0 4.0	~3.7 ~0.4	[75]
Pd -	Carbon deficient g-C_3N_4	n/a n/a	~2.8 ~0.115	[108]
V -	Polymeric C_3N_4	4.6 1.7	~5.0 ~1.5	[55]
Ni -	Sulfur-vacancy-enrich ZnI_2S_4	~22.5 ~10.0	~0.089 ~0.04	[49]
Pt -	ZnI_2S_4 NSs	~17.0 ~4.0	0.35 0.02	[80]
-	$CuInS_2/ZnIn_2S_4$	~0.75	~0.34	[109]
Pt -	$FAPbBr_{3-x}I_x$	~12.0 ~3.0	~0.7 ~0.05	[81]
-	$Cs_3Bi_{0.6}Sb_{1.4}I_9$	~20	n/a	[84]
Pt -	TpPa COF	n/a n/a	~0.72 0.015	[82]
- -	TP-BDDA COF TP-DTP COF	n/a n/a	0.32 0.03	[96]

5. Conclusions and Outlook

The use of single-atom photocatalyst has reached a milestone in terms of its physical and chemical properties, thereby enhancing the performance of the catalyst in HER. In addition, it allows any type of light harvester to become a photocatalyst for hydrogen production, CO_2 reduction, oxygen evolution reaction (OER), or organic oxidation. In order to obtain the superior photocatalyst, various heterogeneous or homogeneous methods are utilized. Various in/ex situ experimental/computational techniques, such as transmission electron microscopy, X-ray photoelectron spectroscopy, X-ray absorption spectroscopy, and DFT calculation, gradually reveal the structure and electronic properties. The mechanism of the photocatalyst is partially revealed. Recorded hydrogen production rates range from hundreds of micro to millimoles per hour. Accordingly, these are significant steps toward the future of producing clean, environmentally friendly fuels.

Despite numerous advancements, the SMA photocatalyst still faces a number of obstacles and requires additional research in areas such as selectivity, metal coordination investigation in practical experiments, stability, and controllable processes. For instance, computational research readily identified the transition metals (Mn, Fe, Co, Ni, Cu, Pd, and Pt) with distinct Gibbs free energy coordination for hydrogen absorption; however, there is still a gap where experimental work can determine the behaviour of transition metals with various coordination [34]. In addition, computational work is necessary to predict and comprehend the behaviour of single-metal atoms on various types of materials. It has been suggested that OHP are highly stable; however, there is a lack of experimental evidence demonstrating how long the material can maintain continuous photocatalytic performance.

The combination of light-harvesting materials with varying absorption ranges can be an effective strategy for using solar light to drive photocatalytic reactions.

In addition, the OER reaction is also a boost-up key for hydrogen evolution reaction due to its counter reaction to HER [110,111]. As the balancing system, the generated electron–hole couple should be effectively separated and join in HER and OER. Therefore, the rate of the overall system is determined based on the rate of HER and OER. Unlike HER, OER works based on oxidation by the valence band of semiconductors [112,113]. Recently, the single atom photocatalyst also shows a great improvement for OERs; therefore, with the same concept, SMA photocatalysts are promising for practical and sustainable environmental devices [114,115]. Solar driven HER and OER by two separated electrodes will be the ideal system, efficiently producing H_2 and O_2. However, they both face the same hurdles to overcome: full investigation, material preparation, and theoretical predictions. The rapid rise of single atoms to the forefront of photocatalyst research demonstrates a promising future for the use of a brand new catalyst material to address a variety of issues, including energy, the environment, and healthcare.

Author Contributions: T.P.N.: Conceptualization, visualization, writing, review, and editing. I.T.K.: project administration, funding acquisition, review, and editing. All authors have read and agreed to the published version of the manuscript.

Funding: This study was supported by a National Research Foundation of Korea (NRF) grant funded by the Korean government (MSIT) (NRF-2022R1F1A1062928). This research was also supported by the Basic Science Research Capacity Enhancement Project through a Korea Basic Science Institute (National Research Facilities and Equipment Center) grant funded by the Ministry of Education (2019R1A6C1010016).

Data Availability Statement: Not applicable.

Conflicts of Interest: The authors declare no conflict of interest.

References

1. Turner, J.; Sverdrup, G.; Mann, M.K.; Maness, P.-C.; Kroposki, B.; Ghirardi, M.; Evans, R.J.; Blake, D. Renewable hydrogen production. *Int. J. Energy Res.* **2008**, *32*, 379–407. [CrossRef]
2. Dubouis, N.; Grimaud, A. The hydrogen evolution reaction: From material to interfacial descriptors. *Chem. Sci.* **2019**, *10*, 9165–9181. [CrossRef] [PubMed]
3. Nguyen, T.P.; Tuan Nguyen, D.M.; Tran, D.L.; Le, H.K.; Vo, D.-V.N.; Lam, S.S.; Varma, R.S.; Shokouhimehr, M.; Nguyen, C.C.; Le, Q.V. MXenes: Applications in electrocatalytic, photocatalytic hydrogen evolution reaction and CO_2 reduction. *Mol. Catal.* **2020**, *486*, 110850. [CrossRef]
4. Wang, X.; Jiang, X.; Sharman, E.; Yang, L.; Li, X.; Zhang, G.; Zhao, J.; Luo, Y.; Jiang, J. Isolating hydrogen from oxygen in photocatalytic water splitting with a carbon-quantum-dot/carbon-nitride hybrid. *J. Mater. Chem. A* **2019**, *7*, 6143–6148. [CrossRef]
5. Lin, S.; Huang, H.; Ma, T.; Zhang, Y. Photocatalytic Oxygen Evolution from Water Splitting. *Adv. Sci.* **2021**, *8*, 2002458. [CrossRef] [PubMed]
6. Dawood, F.; Anda, M.; Shafiullah, G.M. Hydrogen production for energy: An overview. *Int. J. Hydrogen Energy* **2020**, *45*, 3847–3869. [CrossRef]
7. Holladay, J.D.; Hu, J.; King, D.L.; Wang, Y. An overview of hydrogen production technologies. *Catal. Today* **2009**, *139*, 244–260. [CrossRef]
8. Strmcnik, D.; Lopes, P.P.; Genorio, B.; Stamenkovic, V.R.; Markovic, N.M. Design principles for hydrogen evolution reaction catalyst materials. *Nano Energy* **2016**, *29*, 29–36. [CrossRef]
9. Nikolaidis, P.; Poullikkas, A. A comparative overview of hydrogen production processes. *Renew. Sustain. Energy Rev.* **2017**, *67*, 597–611. [CrossRef]
10. Santos, E.; Lundin, A.; Pötting, K.; Quaino, P.; Schmickler, W. Model for the electrocatalysis of hydrogen evolution. *Phys. Rev. B* **2009**, *79*, 235436. [CrossRef]
11. Crawford, S.; Thimsen, E.; Biswas, P. Impact of Different Electrolytes on Photocatalytic Water Splitting. *J. Electrochem. Soc.* **2009**, *156*, H346. [CrossRef]
12. Karimi Estahbanati, M.R.; Mahinpey, N.; Feilizadeh, M.; Attar, F.; Iliuta, M.C. Kinetic study of the effects of pH on the photocatalytic hydrogen production from alcohols. *Int. J. Hydrogen Energy* **2019**, *44*, 32030–32041. [CrossRef]
13. Huang, B.; Rao, R.R.; You, S.; Hpone Myint, K.; Song, Y.; Wang, Y.; Ding, W.; Giordano, L.; Zhang, Y.; Wang, T.; et al. Cation- and pH-Dependent Hydrogen Evolution and Oxidation Reaction Kinetics. *JACS Au* **2021**, *1*, 1674–1687. [CrossRef]

14. Zhang, G.; Zhang, W.; Minakata, D.; Chen, Y.; Crittenden, J.; Wang, P. The pH effects on H_2 evolution kinetics for visible light water splitting over the Ru/$(CuAg)_{0.15}In_{0.3}Zn_{1.4}S_2$ photocatalyst. *Int. J. Hydrogen Energy* **2013**, *38*, 11727–11736. [CrossRef]
15. Anantharaj, S.; Noda, S. Amorphous Catalysts and Electrochemical Water Splitting: An Untold Story of Harmony. *Small* **2020**, *16*, 1905779. [CrossRef]
16. Jerkiewicz, G. Standard and Reversible Hydrogen Electrodes: Theory, Design, Operation, and Applications. *ACS Catal.* **2020**, *10*, 8409–8417. [CrossRef]
17. Xia, Y.; Sayed, M.; Zhang, L.; Cheng, B.; Yu, J. Single-atom heterogeneous photocatalysts. *Chem Catalysis* **2021**, *1*, 1173–1214. [CrossRef]
18. Zhao, W.; Chen, Z.; Yang, X.; Qian, X.; Liu, C.; Zhou, D.; Sun, T.; Zhang, M.; Wei, G.; Dissanayake, P.D.; et al. Recent advances in photocatalytic hydrogen evolution with high-performance catalysts without precious metals. *Renew. Sustain. Energy Rev.* **2020**, *132*, 110040. [CrossRef]
19. Gellé, A.; Moores, A. Water splitting catalyzed by titanium dioxide decorated with plasmonic nanoparticles. *Pure Appl. Chem.* **2017**, *89*, 1817–1827. [CrossRef]
20. Grätzel, M. Photoelectrochemical cells. *Nature* **2001**, *414*, 338–344. [CrossRef]
21. Xia, B.; Zhang, Y.; Ran, J.; Jaroniec, M.; Qiao, S.-Z. Single-Atom Photocatalysts for Emerging Reactions. *ACS Central Science* **2021**, *7*, 39–54. [CrossRef] [PubMed]
22. Hasija, V.; Patial, S.; Raizada, P.; Aslam Parwaz Khan, A.; Asiri, A.M.; Van Le, Q.; Nguyen, V.-H.; Singh, P. Covalent organic frameworks promoted single metal atom catalysis: Strategies and applications. *Coord. Chem. Rev.* **2022**, *452*, 214298. [CrossRef]
23. Wang, Q.; Li, J.; Tu, X.; Liu, H.; Shu, M.; Si, R.; Ferguson, C.T.J.; Zhang, K.A.I.; Li, R. Single Atomically Anchored Cobalt on Carbon Quantum Dots as Efficient Photocatalysts for Visible Light-Promoted Oxidation Reactions. *Chem. Mater.* **2020**, *32*, 734–743. [CrossRef]
24. Li, C.; Baek, J.-B. Recent Advances in Noble Metal (Pt, Ru, and Ir)-Based Electrocatalysts for Efficient Hydrogen Evolution Reaction. *ACS Omega* **2020**, *5*, 31–40. [CrossRef] [PubMed]
25. Li, X.-H.; Baar, M.; Blechert, S.; Antonietti, M. Facilitating room-temperature Suzuki coupling reaction with light: Mott-Schottky photocatalyst for C-C-coupling. *Sci. Rep.* **2013**, *3*, 1743. [CrossRef]
26. Yan, F.; Wang, Y.; Zhang, J.; Lin, Z.; Zheng, J.; Huang, F. Schottky or Ohmic Metal–Semiconductor Contact: Influence on Photocatalytic Efficiency of Ag/ZnO and Pt/ZnO Model Systems. *ChemSusChem* **2014**, *7*, 101–104. [CrossRef]
27. Cheng, C.; Fang, W.-H.; Long, R.; Prezhdo, O.V. Water Splitting with a Single-Atom Cu/TiO_2 Photocatalyst: Atomistic Origin of High Efficiency and Proposed Enhancement by Spin Selection. *JACS Au* **2021**, *1*, 550–559. [CrossRef]
28. Ge, Z.; Fu, B.; Zhao, J.; Li, X.; Ma, B.; Chen, Y. A review of the electrocatalysts on hydrogen evolution reaction with an emphasis on Fe, Co and Ni-based phosphides. *J. Mater. Sci.* **2020**, *55*, 14081–14104. [CrossRef]
29. Wang, X.; Pan, H.; Sun, M.; Zhang, Y. Au single atom-anchored WO_3/TiO_2 nanotubes for the photocatalytic degradation of volatile organic compounds. *J. Mater. Chem. A* **2022**, *10*, 6078–6085. [CrossRef]
30. Hou, T.; Peng, H.; Xin, Y.; Wang, S.; Zhu, W.; Chen, L.; Yao, Y.; Zhang, W.; Liang, S.; Wang, L. Fe Single-Atom Catalyst for Visible-Light-Driven Photofixation of Nitrogen Sensitized by Triphenylphosphine and Sodium Iodide. *ACS Catal.* **2020**, *10*, 5502–5510. [CrossRef]
31. Xiong, X.; Mao, C.; Yang, Z.; Zhang, Q.; Waterhouse, G.I.N.; Gu, L.; Zhang, T. Photocatalytic CO_2 Reduction to CO over Ni Single Atoms Supported on Defect-Rich Zirconia. *Adv. Energy Mater.* **2020**, *10*, 2002928. [CrossRef]
32. Łosiewicz, B.; Popczyk, M.; Napłoszek, I.; Budniok, A. Intermetallic Compounds as Catalysts in the Reaction of Electroevolution/Absorption of Hydrogen. *Solid State Phenom.* **2015**, *228*, 16–22. [CrossRef]
33. Xue, Z.-H.; Luan, D.; Zhang, H.; Lou, X.W. Single-atom catalysts for photocatalytic energy conversion. *Joule* **2022**, *6*, 92–133. [CrossRef]
34. Gao, G.; Bottle, S.; Du, A. Understanding the activity and selectivity of single atom catalysts for hydrogen and oxygen evolution via ab initial study. *Catal. Sci. Technol.* **2018**, *8*, 996–1001. [CrossRef]
35. Zheng, Y.; Jiao, Y.; Jaroniec, M.; Qiao, S.Z. Advancing the Electrochemistry of the Hydrogen-Evolution Reaction through Combining Experiment and Theory. *Angew. Chem. Int. Ed.* **2015**, *54*, 52–65. [CrossRef]
36. Yang, C.; Zhao, Z.-Y.; Wei, H.-T.; Deng, X.-Y.; Liu, Q.-J. DFT calculations for single-atom confinement effects of noble metals on monolayer g-C_3N_4 for photocatalytic applications. *RSC Adv.* **2021**, *11*, 4276–4285. [CrossRef]
37. Zhang, C.; Qin, D.; Zhou, Y.; Qin, F.; Wang, H.; Wang, W.; Yang, Y.; Zeng, G. Dual optimization approach to Mo single atom dispersed g-C_3N_4 photocatalyst: Morphology and defect evolution. *Appl. Catal. B* **2022**, *303*, 120904. [CrossRef]
38. Song, W.; Lv, X.; Gao, Y.; Wang, L. Photocatalytic HER Performance of TiO_2-supported Single Atom Catalyst Based on Electronic Regulation: A DFT Study. *Chem. Res. Chin. Univ.* **2022**, *38*, 1025–1031. [CrossRef]
39. Hammer, B.; Norskov, J.K. Why gold is the noblest of all the metals. *Nature* **1995**, *376*, 238–240. [CrossRef]
40. Santos, E.; Schmickler, W. d-Band Catalysis in Electrochemistry. *ChemPhysChem* **2006**, *7*, 2282–2285. [CrossRef]
41. He, T.; Zhang, C.; Du, A. Single-atom supported on graphene grain boundary as an efficient electrocatalyst for hydrogen evolution reaction. *Chem. Eng. Sci.* **2019**, *194*, 58–63. [CrossRef]
42. Hu, J.; Zhang, C.; Meng, X.; Lin, H.; Hu, C.; Long, X.; Yang, S. Hydrogen evolution electrocatalysis with binary-nonmetal transition metal compounds. *J. Mater. Chem. A* **2017**, *5*, 5995–6012. [CrossRef]

43. Zheng, Y.; Jiao, Y.; Zhu, Y.; Li, L.H.; Han, Y.; Chen, Y.; Du, A.; Jaroniec, M.; Qiao, S.Z. Hydrogen evolution by a metal-free electrocatalyst. *Nat. Commun.* **2014**, *5*, 3783. [CrossRef] [PubMed]
44. Nørskov, J.K.; Bligaard, T.; Logadottir, A.; Kitchin, J.R.; Chen, J.G.; Pandelov, S.; Stimming, U. Trends in the Exchange Current for Hydrogen Evolution. *J. Electrochem. Soc.* **2005**, *152*, J23. [CrossRef]
45. Jaramillo, T.F.; Jørgensen, K.P.; Bonde, J.; Nielsen, J.H.; Horch, S.; Chorkendorff, I. Identification of Active Edge Sites for Electrochemical H_2 Evolution from MoS_2 Nanocatalysts. *Science* **2007**, *317*, 100–102. [CrossRef] [PubMed]
46. Greeley, J.; Nørskov, J.K.; Kibler, L.A.; El-Aziz, A.M.; Kolb, D.M. Hydrogen Evolution Over Bimetallic Systems: Understanding the Trends. *ChemPhysChem* **2006**, *7*, 1032–1035. [CrossRef]
47. Zhang, Y.; Zhao, J.; Wang, H.; Xiao, B.; Zhang, W.; Zhao, X.; Lv, T.; Thangamuthu, M.; Zhang, J.; Guo, Y.; et al. Single-atom Cu anchored catalysts for photocatalytic renewable H_2 production with a quantum efficiency of 56%. *Nat. Commun.* **2022**, *13*, 58. [CrossRef]
48. Cha, G.; Hwang, I.; Hejazi, S.; Dobrota, A.S.; Pašti, I.A.; Osuagwu, B.; Kim, H.; Will, J.; Yokosawa, T.; Badura, Z.; et al. As a single atom Pd outperforms Pt as the most active co-catalyst for photocatalytic H_2 evolution. *iScience* **2021**, *24*, 102938. [CrossRef]
49. Pan, J.; Zhang, G.; Guan, Z.; Zhao, Q.; Li, G.; Yang, J.; Li, Q.; Zou, Z. Anchoring Ni single atoms on sulfur-vacancy-enriched $ZnIn_2S_4$ nanosheets for boosting photocatalytic hydrogen evolution. *J. Energy Chem.* **2021**, *58*, 408–414. [CrossRef]
50. Zhou, K.L.; Wang, Z.; Han, C.B.; Ke, X.; Wang, C.; Jin, Y.; Zhang, Q.; Liu, J.; Wang, H.; Yan, H. Platinum single-atom catalyst coupled with transition metal/metal oxide heterostructure for accelerating alkaline hydrogen evolution reaction. *Nat. Commun.* **2021**, *12*, 3783. [CrossRef]
51. Vilé, G.; Sharma, P.; Nachtegaal, M.; Tollini, F.; Moscatelli, D.; Sroka-Bartnicka, A.; Tomanec, O.; Petr, M.; Filip, J.; Pieta, I.S.; et al. An Earth-Abundant Ni-Based Single-Atom Catalyst for Selective Photodegradation of Pollutants. *Solar RRL* **2021**, *5*, 2100176. [CrossRef]
52. Zhang, P.; Zhan, X.; Xu, L.; Fu, X.; Zheng, T.; Yang, X.; Xu, Q.; Wang, D.; Qi, D.; Sun, T.; et al. Mass production of a single-atom cobalt photocatalyst for high-performance visible-light photocatalytic CO_2 reduction. *J. Mater. Chem. A* **2021**, *9*, 26286–26297. [CrossRef]
53. Zhou, X.; Hwang, I.; Tomanec, O.; Fehn, D.; Mazare, A.; Zboril, R.; Meyer, K.; Schmuki, P. Advanced Photocatalysts: Pinning Single Atom Co-Catalysts on Titania Nanotubes. *Adv. Funct. Mater.* **2021**, *31*, 2102843. [CrossRef]
54. Yang, J.; Sun, Z.; Yan, K.; Dong, H.; Dong, H.; Cui, J.; Gong, X.; Han, S.; Huang, L.; Wen, J. Single-atom-nickel photocatalytic site-selective sulfonation of enamides to access amidosulfones. *Green Chem.* **2021**, *23*, 2756–2762. [CrossRef]
55. Wang, K.; Jiang, L.; Xin, T.; Li, Y.; Wu, X.; Zhang, G. Single-atom V-N charge-transfer bridge on ultrathin carbon nitride for efficient photocatalytic H_2 production and formaldehyde oxidation under visible light. *Chem. Eng. J.* **2022**, *429*, 132229. [CrossRef]
56. Sun, S.; Zhang, G.; Gauquelin, N.; Chen, N.; Zhou, J.; Yang, S.; Chen, W.; Meng, X.; Geng, D.; Banis, M.N.; et al. Single-atom Catalysis Using Pt/Graphene Achieved through Atomic Layer Deposition. *Sci. Rep.* **2013**, *3*, 1775. [CrossRef]
57. Liang, J.; Song, Q.; Wu, J.; Lei, Q.; Li, J.; Zhang, W.; Huang, Z.; Kang, T.; Xu, H.; Wang, P.; et al. Anchoring Copper Single Atoms on Porous Boron Nitride Nanofiber to Boost Selective Reduction of Nitroaromatics. *ACS Nano* **2022**, *16*, 4152–4161. [CrossRef]
58. Schneider, J.; Matsuoka, M.; Takeuchi, M.; Zhang, J.; Horiuchi, Y.; Anpo, M.; Bahnemann, D.W. Understanding TiO_2 Photocatalysis: Mechanisms and Materials. *Chem. Rev.* **2014**, *114*, 9919–9986. [CrossRef]
59. Guo, Q.; Zhou, C.; Ma, Z.; Yang, X. Fundamentals of TiO_2 Photocatalysis: Concepts, Mechanisms, and Challenges. *Adv. Mater.* **2019**, *31*, 1901997. [CrossRef]
60. Song, T.; Paik, U. TiO_2 as an active or supplemental material for lithium batteries. *J. Mater. Chem. A* **2016**, *4*, 14–31. [CrossRef]
61. Cho, H.; Joo, H.; Kim, H.; Kim, J.-E.; Kang, K.-S.; Jung, H.; Yoon, J. Enhanced Photoelectrochemical Activity of TiO_2 Nanotubes Decorated with Lanthanide Ions for Hydrogen Production. *Catalysts* **2022**, *12*, 866. [CrossRef]
62. Son, Y.J.; Kang, J.S.; Yoon, J.; Kim, J.; Jeong, J.; Kang, J.; Lee, M.J.; Park, H.S.; Sung, Y.-E. Influence of TiO_2 Particle Size on Dye-Sensitized Solar Cells Employing an Organic Sensitizer and a Cobalt(III/II) Redox Electrolyte. *J. Phys. Chem. C* **2018**, *122*, 7051–7060. [CrossRef]
63. Nam, Y.; Lim, J.H.; Ko, K.C.; Lee, J.Y. Photocatalytic activity of TiO_2 nanoparticles: A theoretical aspect. *J. Mater. Chem. A* **2019**, *7*, 13833–13859. [CrossRef]
64. Shayegan, Z.; Lee, C.-S.; Haghighat, F. TiO_2 photocatalyst for removal of volatile organic compounds in gas phase – A review. *Chem. Eng. J.* **2018**, *334*, 2408–2439. [CrossRef]
65. Yi, L.; Lan, F.; Li, J.; Zhao, C. Efficient Noble-Metal-Free Co-NG/TiO_2 Photocatalyst for H_2 Evolution: Synergistic Effect between Single-Atom Co and N-Doped Graphene for Enhanced Photocatalytic Activity. *ACS Sustain. Chem. Eng.* **2018**, *6*, 12766–12775. [CrossRef]
66. Cui, J.; Liang, S.; Zhang, J. A multifunctional material of two-dimensional g-C_4N_3/graphene bilayer. *Phys. Chem. Chem. Phys.* **2016**, *18*, 25388–25393. [CrossRef]
67. Chen, J.; Fang, S.; Shen, Q.; Fan, J.; Li, Q.; Lv, K. Recent Advances of Doping and Surface Modifying Carbon Nitride with Characterization Techniques. *Catalysts* **2022**, *12*, 962. [CrossRef]
68. Zuluaga, S.; Liu, L.H.; Shafiq, N.; Rupich, S.M.; Veyan, J.F.; Chabal, Y.J.; Thonhauser, T. Structural band-gap tuning in g-C_3N_4. *Phys. Chem. Chem. Phys.* **2015**, *17*, 957–962. [CrossRef]
69. Hong, Y.; Liu, E.; Shi, J.; Lin, X.; Sheng, L.; Zhang, M.; Wang, L.; Chen, J. A direct one-step synthesis of ultrathin g-C_3N_4 nanosheets from thiourea for boosting solar photocatalytic H2 evolution. *Int. J. Hydrogen Energy* **2019**, *44*, 7194–7204. [CrossRef]

70. Antil, B.; Kumar, L.; Ranjan, R.; Shenoy, S.; Tarafder, K.; Gopinath, C.S.; Deka, S. One-Dimensional Multichannel g-$C_3N_{4.7}$ Nanostructure Realizing an Efficient Photocatalytic Hydrogen Evolution Reaction and Its Theoretical Investigations. *ACS Appl. Energy Mater.* **2021**, *4*, 3118–3129. [CrossRef]
71. Majdoub, M.; Anfar, Z.; Amedlous, A. Emerging Chemical Functionalization of g-C_3N_4: Covalent/Noncovalent Modifications and Applications. *ACS Nano* **2020**, *14*, 12390–12469. [CrossRef]
72. Wang, X.; Chen, X.; Thomas, A.; Fu, X.; Antonietti, M. Metal-Containing Carbon Nitride Compounds: A New Functional Organic–Metal Hybrid Material. *Adv. Mater.* **2009**, *21*, 1609–1612. [CrossRef]
73. Thomas, A.; Fischer, A.; Goettmann, F.; Antonietti, M.; Müller, J.-O.; Schlögl, R.; Carlsson, J.M. Graphitic carbon nitride materials: Variation of structure and morphology and their use as metal-free catalysts. *J. Mater. Chem.* **2008**, *18*, 4893–4908. [CrossRef]
74. Cao, Y.; Wang, D.; Lin, Y.; Liu, W.; Cao, L.; Liu, X.; Zhang, W.; Mou, X.; Fang, S.; Shen, X.; et al. Single Pt Atom with Highly Vacant d-Orbital for Accelerating Photocatalytic H_2 Evolution. *ACS Appl. Energy Mater.* **2018**, *1*, 6082–6088. [CrossRef]
75. Li, W.; Li, W.; Guo, Z.; Song, Y.; Tang, S.; Ma, Y.; Xing, X.; Wang, Q. Synthesis of Atomically Thin g-C_3N_4 Nanosheets via Supercritical CO_2 Doping with Single-Atom Cobalt for Photocatalytic Hydrogen Evolution. *ACS Appl. Mater. Interfaces* **2021**, *13*, 52560–52570. [CrossRef]
76. Serpone, N.; Emeline, A.V. Semiconductor Photocatalysis — Past, Present, and Future Outlook. *J. Phys. Chem. Lett.* **2012**, *3*, 673–677. [CrossRef]
77. Li, W.; Lin, Z.; Yang, G. A 2D self-assembled $MoS_2/ZnIn_2S_4$ heterostructure for efficient photocatalytic hydrogen evolution. *Nanoscale* **2017**, *9*, 18290–18298. [CrossRef]
78. Jiao, X.; Chen, Z.; Li, X.; Sun, Y.; Gao, S.; Yan, W.; Wang, C.; Zhang, Q.; Lin, Y.; Luo, Y.; et al. Defect-Mediated Electron-Hole Separation in One-Unit-Cell $ZnIn_2S_4$ Layers for Boosted Solar-Driven CO_2 Reduction. *J. Am. Chem. Soc.* **2017**, *139*, 7586–7594. [CrossRef]
79. Yang, W.; Zhang, L.; Xie, J.; Zhang, X.; Liu, Q.; Yao, T.; Wei, S.; Zhang, Q.; Xie, Y. Enhanced Photoexcited Carrier Separation in Oxygen-Doped $ZnIn_2S_4$ Nanosheets for Hydrogen Evolution. *Angew. Chem. Int. Ed.* **2016**, *55*, 6716–6720. [CrossRef]
80. Shi, X.; Dai, C.; Wang, X.; Hu, J.; Zhang, J.; Zheng, L.; Mao, L.; Zheng, H.; Zhu, M. Protruding Pt single-sites on hexagonal $ZnIn_2S_4$ to accelerate photocatalytic hydrogen evolution. *Nat. Commun.* **2022**, *13*, 1287. [CrossRef]
81. Wu, Y.; Wu, Q.; Zhang, Q.; Lou, Z.; Liu, K.; Ma, Y.; Wang, Z.; Zheng, Z.; Cheng, H.; Liu, Y.; et al. An organometal halide perovskite supported Pt single-atom photocatalyst for H_2 evolution. *Energy Environ. Sci.* **2022**, *15*, 1271–1281. [CrossRef]
82. Dong, P.; Wang, Y.; Zhang, A.; Cheng, T.; Xi, X.; Zhang, J. Platinum Single Atoms Anchored on a Covalent Organic Framework: Boosting Active Sites for Photocatalytic Hydrogen Evolution. *ACS Catal.* **2021**, *11*, 13266–13279. [CrossRef]
83. Kojima, A.; Teshima, K.; Shirai, Y.; Miyasaka, T. Organometal halide perovskites as visible-light sensitizers for photovoltaic cells. *J. Am. Chem. Soc.* **2009**, *131*, 6050–6051. [CrossRef] [PubMed]
84. Chen, G.; Wang, P.; Wu, Y.; Zhang, Q.; Wu, Q.; Wang, Z.; Zheng, Z.; Liu, Y.; Dai, Y.; Huang, B. Lead-Free Halide Perovskite $Cs_3Bi_{2x}Sb_{2-2x}I_9$ ($x \approx 0.3$) Possessing the Photocatalytic Activity for Hydrogen Evolution Comparable to that of $(CH_3NH_3)PbI_3$. *Adv. Mater.* **2020**, *32*, 2001344. [CrossRef] [PubMed]
85. Wang, X.; Wang, H.; Zhang, H.; Yu, W.; Wang, X.; Zhao, Y.; Zong, X.; Li, C. Dynamic Interaction between Methylammonium Lead Iodide and TiO_2 Nanocrystals Leads to Enhanced Photocatalytic H_2 Evolution from HI Splitting. *ACS Energy Lett.* **2018**, *3*, 1159–1164. [CrossRef]
86. Wang, H.; Wang, X.; Chen, R.; Zhang, H.; Wang, X.; Wang, J.; Zhang, J.; Mu, L.; Wu, K.; Fan, F.; et al. Promoting Photocatalytic H_2 Evolution on Organic–Inorganic Hybrid Perovskite Nanocrystals by Simultaneous Dual-Charge Transportation Modulation. *ACS Energy Lett.* **2019**, *4*, 40–47. [CrossRef]
87. Guo, Y.; Liu, G.; Li, Z.; Lou, Y.; Chen, J.; Zhao, Y. Stable Lead-Free $(CH_3NH_3)_3Bi_2I_9$ Perovskite for Photocatalytic Hydrogen Generation. *ACS Sustain. Chem. Eng.* **2019**, *7*, 15080–15085. [CrossRef]
88. Romani, L.; Malavasi, L. Solar-Driven Hydrogen Generation by Metal Halide Perovskites: Materials, Approaches, and Mechanistic View. *ACS Omega* **2020**, *5*, 25511–25519. [CrossRef]
89. Ricciarelli, D.; Kaiser, W.; Mosconi, E.; Wiktor, J.; Ashraf, M.W.; Malavasi, L.; Ambrosio, F.; De Angelis, F. Reaction Mechanism of Photocatalytic Hydrogen Production at Water/Tin Halide Perovskite Interfaces. *ACS Energy Lett.* **2022**, *7*, 1308–1315. [CrossRef]
90. Yu, J.; Xu, X. Expediting H_2 Evolution over $MAPbI_3$ with a Nonnoble Metal Cocatalyst Mo_2C under Visible Light. *Energy Mater. Adv.* **2022**, *2022*, 9836095. [CrossRef]
91. Zhou, P.; Chen, H.; Chao, Y.; Zhang, Q.; Zhang, W.; Lv, F.; Gu, L.; Zhao, Q.; Wang, N.; Wang, J.; et al. Single-atom Pt-I_3 sites on all-inorganic Cs_2SnI_6 perovskite for efficient photocatalytic hydrogen production. *Nat. Commun.* **2021**, *12*, 4412. [CrossRef]
92. Ding, S.Y.; Gao, J.; Wang, Q.; Zhang, Y.; Song, W.G.; Su, C.Y.; Wang, W. Construction of covalent organic framework for catalysis: Pd/COF-LZU1 in Suzuki-Miyaura coupling reaction. *J. Am. Chem. Soc.* **2011**, *133*, 19816–19822. [CrossRef]
93. Cui, K.; Zhong, W.; Li, L.; Zhuang, Z.; Li, L.; Bi, J.; Yu, Y. Well-Defined Metal Nanoparticles@Covalent Organic Framework Yolk–Shell Nanocages by ZIF-8 Template as Catalytic Nanoreactors. *Small* **2019**, *15*, 1804419. [CrossRef]
94. Lu, S.; Hu, Y.; Wan, S.; McCaffrey, R.; Jin, Y.; Gu, H.; Zhang, W. Synthesis of Ultrafine and Highly Dispersed Metal Nanoparticles Confined in a Thioether-Containing Covalent Organic Framework and Their Catalytic Applications. *J. Am. Chem. Soc.* **2017**, *139*, 17082–17088. [CrossRef]
95. Zhong, W.; Sa, R.; Li, L.; He, Y.; Li, L.; Bi, J.; Zhuang, Z.; Yu, Y.; Zou, Z. A Covalent Organic Framework Bearing Single Ni Sites as a Synergistic Photocatalyst for Selective Photoreduction of CO_2 to CO. *J. Am. Chem. Soc.* **2019**, *141*, 7615–7621. [CrossRef]

96. Pachfule, P.; Acharjya, A.; Roeser, J.; Langenhahn, T.; Schwarze, M.; Schomacker, R.; Thomas, A.; Schmidt, J. Diacetylene Functionalized Covalent Organic Framework (COF) for Photocatalytic Hydrogen Generation. *J. Am. Chem. Soc.* **2018**, *140*, 1423–1427. [CrossRef]
97. Stegbauer, L.; Schwinghammer, K.; Lotsch, B.V. A hydrazone-based covalent organic framework for photocatalytic hydrogen production. *Chem. Sci.* **2014**, *5*, 2789–2793. [CrossRef]
98. Chai, S.; Chen, X.; Zhang, X.; Fang, Y.; Sprick, R.S.; Chen, X. Rational design of covalent organic frameworks for efficient photocatalytic hydrogen peroxide production. *Environ. Sci. Nano* **2022**, *9*, 2464–2469. [CrossRef]
99. Li, C.; Liu, J.; Li, H.; Wu, K.; Wang, J.; Yang, Q. Covalent organic frameworks with high quantum efficiency in sacrificial photocatalytic hydrogen evolution. *Nat. Commun.* **2022**, *13*, 2357. [CrossRef]
100. Li, X.; Kawai, K.; Fujitsuka, M.; Osakada, Y. COF-based photocatalyst for energy and environment applications. *Surf. Interfaces* **2021**, *25*, 101249. [CrossRef]
101. Wang, S.; Zhang, J.-J.; Zong, M.-Y.; Xu, J.; Wang, D.-H.; Bu, X.-H. Energy Level Engineering: Ru Single Atom Anchored on Mo-MOF with a $[Mo_8O_{26}(im)_2]_4-$ Structure Acts as a Biomimetic Photocatalyst. *ACS Catal.* **2022**, *12*, 7960–7974. [CrossRef]
102. Ma, X.; Yong, X.; Jian, C.-c.; Zhang, J. Transition Metal-Functionalized Janus MoSSe Monolayer: A Magnetic and Efficient Single-Atom Photocatalyst for Water-Splitting Applications. *J. Phys. Chem. C* **2019**, *123*, 18347–18354. [CrossRef]
103. Han, A.; Zhou, X.; Wang, X.; Liu, S.; Xiong, Q.; Zhang, Q.; Gu, L.; Zhuang, Z.; Zhang, W.; Li, F.; et al. One-step synthesis of single-site vanadium substitution in 1T-WS_2 monolayers for enhanced hydrogen evolution catalysis. *Nat. Commun.* **2021**, *12*, 709. [CrossRef] [PubMed]
104. Wang, X.; Zhang, Y.; Si, H.; Zhang, Q.; Wu, J.; Gao, L.; Wei, X.; Sun, Y.; Liao, Q.; Zhang, Z.; et al. Single-Atom Vacancy Defect to Trigger High-Efficiency Hydrogen Evolution of MoS_2. *J. Am. Chem. Soc.* **2020**, *142*, 4298–4308. [CrossRef] [PubMed]
105. Jiang, K.; Liu, B.; Luo, M.; Ning, S.; Peng, M.; Zhao, Y.; Lu, Y.-R.; Chan, T.-S.; de Groot, F.M.F.; Tan, Y. Single platinum atoms embedded in nanoporous cobalt selenide as electrocatalyst for accelerating hydrogen evolution reaction. *Nat. Commun.* **2019**, *10*, 1743. [CrossRef]
106. Luo, Y.; Zhang, S.; Pan, H.; Xiao, S.; Guo, Z.; Tang, L.; Khan, U.; Ding, B.-F.; Li, M.; Cai, Z.; et al. Unsaturated Single Atoms on Monolayer Transition Metal Dichalcogenides for Ultrafast Hydrogen Evolution. *ACS Nano* **2020**, *14*, 767–776. [CrossRef]
107. Lv, S.; Pei, M.; Liu, Y.; Si, Z.; Wu, X.; Ran, R.; Weng, D.; Kang, F. An isolation strategy to anchor atomic Ni or Co cocatalysts on TiO_2(A) for photocatalytic hydrogen production. *Nano Res.* **2022**, *15*, 5848–5856. [CrossRef]
108. Liu, G.; Lv, H.; Zeng, Y.; Yuan, M.; Meng, Q.; Wang, Y.; Wang, C. Single-Atom Pd–N3 Sites on Carbon-Deficient g-C3N4 for Photocatalytic H_2 Evolution. *Trans. Tianjin Univ.* **2021**, *27*, 139–146. [CrossRef]
109. Guan, Z.; Pan, J.; Li, Q.; Li, G.; Yang, J. Boosting Visible-Light Photocatalytic Hydrogen Evolution with an Efficient $CuInS_2/ZnIn_2S_4$ 2D/2D Heterojunction. *ACS Sustain. Chem. Eng.* **2019**, *7*, 7736–7742. [CrossRef]
110. Ding, C.; Shi, J.; Wang, Z.; Li, C. Photoelectrocatalytic Water Splitting: Significance of Cocatalysts, Electrolyte, and Interfaces. *ACS Catal.* **2017**, *7*, 675–688. [CrossRef]
111. Li, D.; Liu, Y.; Shi, W.; Shao, C.; Wang, S.; Ding, C.; Liu, T.; Fan, F.; Shi, J.; Li, C. Crystallographic-Orientation-Dependent Charge Separation of $BiVO_4$ for Solar Water Oxidation. *ACS Energy Lett.* **2019**, *4*, 825–831. [CrossRef]
112. Sun, H.; Hua, W.; Li, Y.; Wang, J.-G. Conformal coating of superhydrophilic metal-organic complex toward substantially improved photoelectrochemical water oxidation. *Chem. Eng. J.* **2022**, *427*, 131004. [CrossRef]
113. Sun, H.; Hua, W.; Liang, S.; Li, Y.; Wang, J.-G. A self-adaptive semiconductor–liquid junction for highly active and stable solar water splitting. *J. Mater. Chem. A* **2022**, *10*, 20414–20423. [CrossRef]
114. Lee, W.H.; Ko, Y.-J.; Kim, J.-Y.; Min, B.K.; Hwang, Y.J.; Oh, H.-S. Single-atom catalysts for the oxygen evolution reaction: Recent developments and future perspectives. *Chem. Commun.* **2020**, *56*, 12687–12697. [CrossRef]
115. Yin, J.; Jin, J.; Lu, M.; Huang, B.; Zhang, H.; Peng, Y.; Xi, P.; Yan, C.H. Iridium Single Atoms Coupling with Oxygen Vacancies Boosts Oxygen Evolution Reaction in Acid Media. *J. Am. Chem. Soc.* **2020**, *142*, 18378–18386. [CrossRef]